



Ocean processes south of the Drygalski Ice Tongue, western Ross Sea



Craig Stevens^{a,b,*}, Seung-Tae Yoon^{c,d}, Christopher J. Zappa^e, Una Kim Miller^e, Xianwei Wang^f, Fiona Elliott^a, Liv Cornelissen^{a,b}, Choon-Ki Lee^d, Sukyoung Yun^d, Won Sang Lee^d

^a National Institute of Water and Atmospheric Research, Wellington, New Zealand

^b Dept. Physics, University of Auckland, New Zealand

^c Kyungpook National University, Republic of Korea

^d Korea Polar Research Institute, Yeonsu-gu, Incheon, Republic of Korea

^e Lamont Doherty Earth Observatory of Columbia University, Palisades, NY, USA

^f School of Oceanography, Shanghai Jiao Tong University, Shanghai, China

ARTICLE INFO

Handling Editor: Dr W Smith

Keywords:
Convection
Sea ice
Katabatic wind
Oceanography
Antarctica
High salinity shelf water
Polynya

ABSTRACT

We describe the first year-long hydrographic mooring timeseries from a location just to the south of the Drygalski Ice Tongue – the ice margin that forms the southern boundary of the Terra Nova Bay Polynya in the western Ross Sea. The region is where any northward flowing component of the Victoria Land Coastal Current encounters the ice tongue and supports an occasional polynya. The hydrographic mooring was deployed nearby Geikie Inlet from February 2017 through to March 2018, and was coupled with several contemporaneous oceanographic moorings to the north of the Drygalski Ice Tongue. This provides data with which to examine the water column dynamics in the context of local circulation and interaction with the ice tongue. The Terra Nova Bay region is subject to strong katabatic winds, however the polynya to the south of the Drygalski Ice Tongue operates at different times through the annual cycle when compared to the Terra Nova Bay Polynya to the north, as the sea ice in the south-side region is far more constrained in its motion yet, temperature and salinity are broadly consistent north and south of the ice tongue. Sub-surface Ice Shelf Water is observed south of the ice tongue. Transients in near-bed temperature and salinity are observed on both sides of the ice tongue, albeit with the northside leading by ~8–9 days. Notably, the temperature transient precedes that of salinity by around 40 days. This suggests that, at this near-coastal position, the circulation beneath the ice tongue is primarily southward.

1. Introduction

Ocean processes in the waters around Antarctica are critical for the formation of Antarctic Bottom Water via a polynya-driven salt flux (Orsi et al., 1999; Budillon et al., 2002), as well as contributing to meteoric ice melt where relatively warm seawater comes in contact with ice shelves and ice tongues (Schodlok et al., 2016; Stewart et al., 2019; Friedrichs et al., 2022). Despite the relatively small area given over to these processes in global terms, they provide a localized connection between the atmosphere, cryosphere and ocean that has implications at local, regional and global scales (Morales Maqueda et al., 2004; Bennetts et al., 2024).

In Antarctic coastal waters, at the local scale, katabatic winds blow off the land or fringing ice shelves, advecting pre-existing sea ice, cooling the surface ocean until it is sufficiently cold to change phase and

form nascent sea ice, which is then too advected offshore to form consolidated sea ice (Kusahara et al., 2010). At the regional scale, the sea ice is advected and aggregates in patterns controlled by regional scale winds, topography, Coriolis, ocean currents and its own mechanical strength (Mathiot et al., 2012). This influences sea ice production (Tamura et al., 2016), and in doing so, feeds-back on regional ocean thermodynamics (Cappelletti et al., 2010; Miller et al., 2024a, 2024b) and is a major influence on the regional marine ecosystem (Lizotte, 2001).

Here we look at ocean properties in a coastal setting with both an ice tongue and polynyas. The ice formation process results in salt being excluded from the seawater into the surface ocean which is destabilizing and causes convective plumes to sink through the water column (Williams et al., 2008). This denser, oxygenated, salt-enriched high salinity shelf water (HSSW) –aggregates and flows according to buoyancy,

* Corresponding author. National Institute of Water and Atmospheric Research, Wellington, New Zealand.

E-mail address: craig.stevens@niwa.co.nz (C. Stevens).

bathymetry and the Coriolis force (Williams et al., 2008). This water is transported southward beneath ice shelves where, despite their cold origins, the water is warmer than the local glacial melting temperatures and so drives ice shelf basal melting (Schodlok et al., 2016). At the same time, northward HSSW flow drains off the Antarctic continental shelf and enters the global thermohaline systems (Orsi et al., 1999; Bowen et al., 2021). There are indications that this flux is changing (Gunn et al., 2023).

The oceanic connections between ice tongue basal melting, polynya mechanics, and regional and global outcomes are not well-understood (Rintoul, 2018), and so remains a challenge for modelling approaches (Xu et al., 2023). For example, the Terra Nova Bay Polynya (TNBP) region in the Western Ross Sea (Fig. 1) is typically only 60×40 km in areal extent – although this area is highly variable (Ciappa et al., 2012; Aulicino et al., 2018). Despite this, the TNBP is considered important in global budgets of both sea ice and Antarctic bottom water production. The TNBP itself has been the focus of a substantial body of work where phenomena examined range from air-sea interaction in katabatic-driven conditions (Fusco et al., 2009), sea ice (Sansiviero et al., 2017) and HSSW production (Mathiot et al., 2012; Yoon et al., 2020; Miller et al., 2024a).

It has been suggested that the region is responsible for around 3% of Antarctic polynya-produced sea ice production (Tamura et al., 2016) and as much as 10% of Antarctic Bottom Water (van Woert, 1999; Orsi et al., 2002). The high sea ice production rate in the TNBP is made possible because of the confluence of strong katabatic winds and the presence of the 90 km long floating extension of the David Glacier, the Drygalski Ice Tongue (DIT). The DIT is the largest free-floating glacier in Antarctica at present (Frezzotti and Mabin, 1994). This substantial cryptography blocks sea ice advection from the south (Gomez-Fell et al., 2023).

What is yet to be understood for the TNBP region is the connection to the region to the south of the ice tongue, as, apart from a summer-snapshot (Stevens et al., 2017), there has been little oceanographic work in the region just to the south of the DIT. Here we examine a year-long hydrographic record from south of the DIT (Fig. 1) to explore how the region is connected to the ice tongue and the Terra Nova Bay polynya to the north of the ice tongue. Critically, examination of satellite inferred melt rate identifies a clear north-south difference for the

Drygalski Ice Tongue (Fig. 2) with greater melt rates to the south. Oceanographically, the DIT is regarded as a south-to-north transition point whereby the south side can potentially be affected by buoyant Ice Shelf Water (ISW) outflows from the large Ross Ice Shelf 300 km to the south (Stevens et al., 2017). Robinson et al. (2014) identified north-flowing ISW against the Victoria Land coast in McMurdo Sound and with studies proposing the persistence of this current northwards was controlled either through mixing (Stevens et al., 2009) or platelet ice crystal processes (Hughes et al., 2014; Robinson et al., 2014). It was expected that ISW observed by Robinson et al. (2014) in McMurdo Sound would accumulate on the south side of the DIT. This was apparent in the surface water of the summer DIT hydrographic survey described in Stevens et al. (2017) but the hydrography was poorly correlated below the surface layer and is at odds with the satellite melt rates (Fig. 2). Here we examine a year-long hydrographic dataset with a focus on the water column dynamics in the region to the south of the DIT through the annual cycle and the influence of the local polynya and ice tongue and how it might connect with TNBP. This motivates several questions. What controls the water column dynamics south of the DIT? Is there a north-south connection? What are the regional implications due to the south-side ocean conditions?

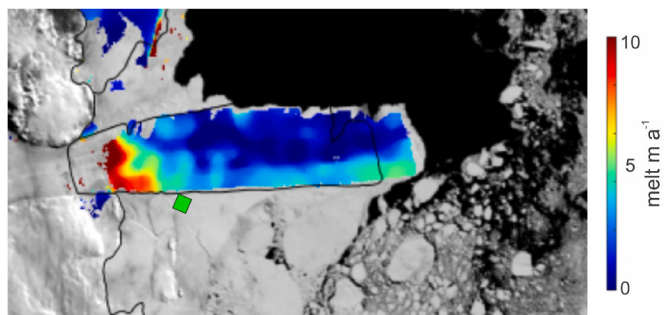


Fig. 2. Spatial distribution of estimated melt rate from Adusumilli et al. (2020). Green square is DITS location.

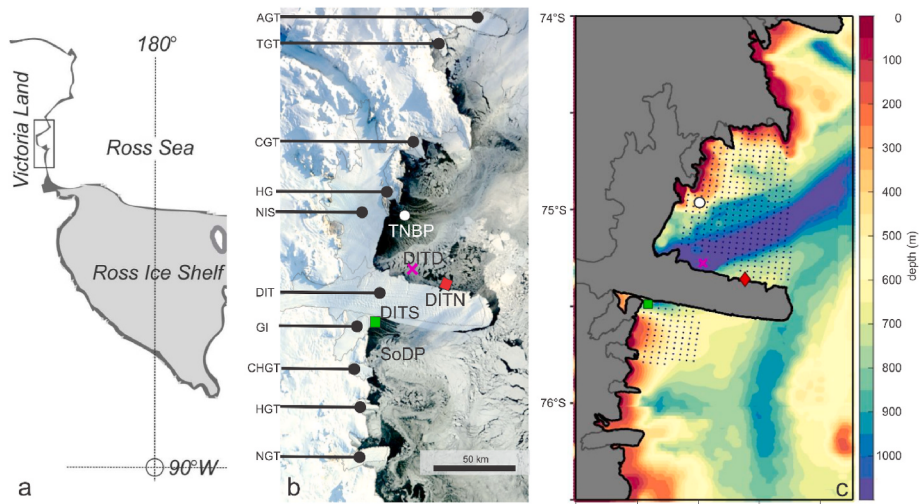


Fig. 1. Location details showing (a) Ross/Victoria Land sector with the focal region boxed, (b) Central Victoria Land coast centered about the Drygalski Ice Tongue (DIT) and the TNBP. Other glacier tongues include Aviator (AGT), Tinker (TGT), Campbell (CGT), Cheetham (CHGT), Harbord (HGT) and Nordenskjöld (NGT). Additional features include the Nansen Ice Shelf (NIS), Hells Gate (HG), South Drygalski Polynya (SoDP) and Geike Inlet (GI). The underlying MODIS image was acquired on the March 22, 2017. Sampling stations DITN, DITS and DITD are also marked along with the mooring (white circle) described in Miller et al. (2024a). (c) The surveyed bathymetry (merged with the IBCSO product) and the area interrogated for sea ice coverage (dots correspond to ARTIST pixels) for the analysis described in Fig. 3b.

2. Methods

2.1. Location

The central Victoria Land coastal region between latitudes 74°S and 77°S is dominated by the ~90 km long Drygalski Ice Tongue (Fig. 1). Recent estimation of the grounding line position suggests it occurs at a depth of around 1900 m (Indrigo et al., 2021), and 50 km upstream from the wider coast. The DIT is around 300 m thick at its tip, in only 600 m of water depth. The water column deepens to over 1200 m depth moving towards the coast due to the Drygalski basin (Fig. 1C). The DIT provides the southern boundary of the Nansen Ice Shelf which covers a small ocean cavity (Dow et al., 2018; Indrigo et al., 2021). Just to the south of the DIT, as revealed in satellite imagery, is what we label here as the South Drygalski Polynya (SoDP), offshore of Geikie Inlet (not to be confused with a place with the same name in the Arctic). Further south there are a sequence of smaller (although still large), oceanographically unexplored ice shelves and glacier/ice tongues (Fig. 1) exhibiting a range of melt rates and polynya/ice interactions (Gomez-Fell et al., 2023).

2.2. Hydrographic data

Three hydrographic moorings were maintained over the majority of the 2017 year and into early 2018 (Table 1) from the ice breaking research vessel IBRV Araon (Korea Polar Research Institute, KOPRI). The moorings are “Drygalski Ice Tongue-South” (DITS) located south of the ice tongue and to the north the “Drygalski Ice Tongue-North” (DITN) and “Drygalski Ice Tongue-Deep” (DITD) where the latter is a near bed sensor in the trough running north from the glacier (Fig. 1). Yoon et al. (2020) and Miller et al. (2024b) describe the northern data in the context of HSSW production, while here we provide the first presentation of the DITS records. The moorings support temperature-salinity-pressure (SBE37SM Sea-Bird Scientific and presented here in TEOS-10 units), and ocean current sensors (a mix of Aanderaa RCM9 and Nortek Aquadopp) at three depths (see Table 1). The magnetic declination offset (~136°) was applied to the current direction. The temperature and salinity values obtained from these moorings were validated and corrected with conductivity-temperature-depth (CTD – Seabird Electronics SBE 911 plus) profiles in the moorings’ position at deployment and recovery.

In order to gather near-surface data, the hydrographic moorings had relatively shallow upper sensors and floatation for an Antarctic mooring (which typically do not have instruments shallower than 250 m to avoid icebergs). A mooring two years prior (and to the east of the DITS, i.e. due south of DITN) was not locatable (no response from acoustic release and no presence in acoustic survey). In addition, the moorings were located very close to the ice tongue to provide focus on the glacier effect on the nearby ocean. The DITS location is rarely sea ice free.

A consequence of sea ice operational requirements at the time of deployment was that the DITS mooring was placed at a location of greater depth than intended and so the sensors were not at the same

depth as DITN (the DITS upper and middle sensors are around 100 m deeper than the DITN equivalents). Furthermore, the deep DITD is located 500 m deeper than the DITN bottom instrument (Table 1) in order to monitor drainage of HSSW. In addition, in supercooled water associated with ice shelf melt it is possible that temperature and conductivity sensors readings are compromised due to ice crystal formation (Robinson et al., 2020). However, the dynamic range of the salinity signals suggests that the instruments remained unaffected by this (see later).

2.3. Sea ice and wind

The ARTIST (Arctic Radiation and Turbulence Interaction Study) sea-ice products provide an estimate of polynya area by identifying sea ice free regions using the daily (Yoon et al., 2020). This has a grid cell spacing of 3.125 km from the Advanced Microwave Scanning Radiometer 2 data set (Spreen et al., 2008). We applied the same continental masking obtained from the recent data and defined regions of sea ice concentrations below 20% as open water (Parkinson et al., 1999).

Three-hourly 10 m wind and 2 m air temperature data is provided by the ERA-Interim reanalysis dataset (Dee et al., 2011). A grid cell size for ERA-Interim data is $0.75^\circ \times 0.75^\circ$ and so is a spatially smoothed product with a grid cell that is generally too coarse to resolve steep glacier slopes, which may be the reason for the large difference in wind speed compared to observed data (Fusco et al., 2002; Yoon et al., 2020). While it mostly fails to capture katabatic events (Miller et al., 2024a), it is however indicative of wind variability.

3. Results

3.1. Wind and polynya

A synthesis of the key atmosphere-ice-ocean timeseries (Fig. 3) through the 2017 year shows stronger winds in the March–September period, with some strong transient spikes (Fig. 3a). Clearly, the ERA underestimates observed wind speeds (Jones et al., 2016), despite this, at the broad scales this correlates with the open water areas (Fig. 3b) which highlights some differences, in terms of timing, between the two polynyas. The Southern Drygalski Polynya area is only sporadically ice-free, except for a contiguous period in March–April (Fig. 3b) and which can also be seen in the analysis of Aulicino et al. (2018). This is different to the TNBP region, which is fully open from November–February (assuming year-to-year consistency). There are some limits to the approach as (i) the areal maximum is a function of the number of pixels interrogated and (ii) an open water pixel in the ARTIST analysis does not necessarily indicate an operating polynya actively producing sea ice in that pixel.

Considering the Drygalski south-side sea ice (Fig. 4), we examine if the offshore sea ice field relates to the polynya operation. The correlation coefficient between time series of Southern Drygalski Polynya area and offshore sea ice coverage is -0.77 , indicating that polynya development favours periods when sea ice concentration in the offshore region is relatively low.

3.2. Hydrographic timeseries

A comparison of hydrographic timeseries either side of the DIT through depth and time (Fig. 5) shows moderate consistency in structure and absolute values. The summer surface warming was primarily only to the north (Fig. 5a), salinity however was similar at DITN and DITS mooring stations with a minimum in the austral summer-autumn transition that was earlier at shallow depths. ISW observed in McMurdo Sound was around $\Theta = -1.91^\circ\text{C}$ and $S_A = 34.8\text{ g/kg}$ (Robinson et al., 2014) and should accumulate on the south side of the DIT. Temperature at upper and mid depths at the DITS (Fig. 5f and g) station had clear evidence of Ice Shelf Water influence. The mid-water instrument at DITS

Table 1
Mooring locations.

	DITN	DITD	DITS
Location	Drygalski Ice Tongue North	Drygalski Ice Tongue Deep	Drygalski Ice Tongue South
Latitude	75° 21.646' S	75° 16.542' S	75° 29.305' S
Longitude	164° 44.788' E	164° 4.038' E	163° 10.461' E
Water depth (m)	673	1216	1080
Start yyyy/mm/dd	2017/02/09	2017/02/08	2017/02/12
Deployment duration (days)	390.5	390.5	386
Instrument depths (dbar)	75, 275, 675.	1224.	192, 379., 1088.

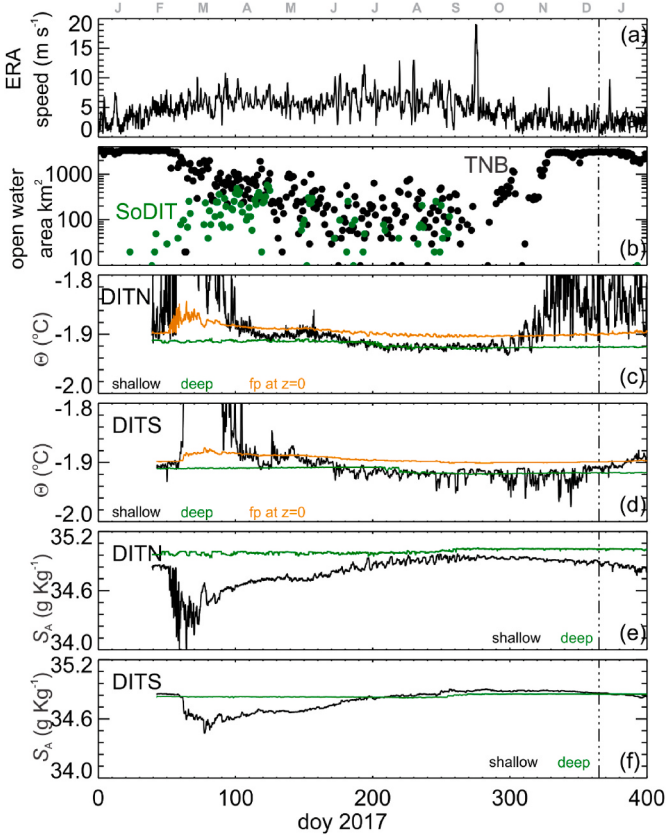


Fig. 3. 2017 timeseries showing (a) ERA wind speed, (b) north and south open water area, (c) DITN temperatures, (d) DITS temperatures, (e) DITN salinities, (f) DITS salinities. DITN sensors depths are upper (75 dbar) and lower (675 dbar) while DITS sensor depths are upper (192 dbar) and lower (1088 dbar).

(379 m) dropped to ~ 0.1 °C below surface freezing (i.e. supercooling). The near-bed temperature and salinity had more in common with other near-bed stations despite the 550 m difference in sensor depths (Fig. 5c, d, g).

The summertime open waters in TNB (Fig. 3a) resulted in warm upper ocean temperatures at DITN (Fig. 3c), but by late April the surface ocean had cooled. Despite this, there was clear separation in temperatures between upper and deeper temperatures until early July – a condition that was maintained until November, at which point the annual cycle presumably repeats. The situation was similar at DITS for the first part of the year but (i) there were strong supercooling events throughout June–December (Fig. 5 f) as seen when the temperature drops below the

surface freezing level. Furthermore, (ii) the surface warming didn't appear to start until February (Fig. 3d; Fig. 5 e). The salinity structures at DITN and DITS (Fig. 3e and f; Fig. 5) are consistent with the temperature structure with an abrupt surface freshening commences around March that then gradually decays through the year but always staying fresher than the almost invariant deeper waters. A notable difference was that the upper sensor salinity was more variable at DITN, most likely because the sensors were 120 m shallower.

Viewing the temperature-salinity distributions in the same layout (Fig. 6), now with a seasonal colour-scaling, the summer-autumn surface warming is the most apparent especially at DITN. Budillon and Spezie (2000) identified several water masses in the TNBP region (presented here in TEOS-10 units) including summer surface water ($-1.7 < \Theta < 1.5$ °C, $33.2 < S_A < 34.7$ g kg⁻¹), Terra Nova Bay Ice Shelf Water (TNBISW; $\Theta < -1.92$ °C, $34.9 < S_A < 35.0$ g kg⁻¹) and HSSW ($\Theta \sim -1.91$ °C, $34.9 < S_A < 35.0$ g kg⁻¹). Trends in salinity are described by Castagno et al. (2019). Here, we identified both TNBISW and HSSW at lower salinities. The shallow upper DITN sensor affords us the opportunity to measure even warmer summer water which reached almost -1.0 °C. All the deeper sensors see HSSW (or possibly TNBISW in the case of DITN) almost continually. The summer surface water potentially contained meltwater input and so supports a “buoyant wedge” similar to that seen off the Ross Ice Shelf (Malyarenko et al., 2019). The “hook-like” features in the range of summer surface waters relate to freshwater inputs by ice-front melting in the austral summer and is similar to structure observed in front of the Ross Ice Shelf (Malyarenko et al., 2019; Stewart et al., 2019). Here this is seen in autumn at DITS and summer and autumn at DITN (Fig. 6) although this might also be related to the deeper sampling point at DITS.

In terms of temperature-salinity water masses, Category One in Fig. 6 is a transitional stage to summer surface water, in the range 34.6–34.75 g kg⁻¹ and conservative temperatures in the range -1.65 to -1.85 °C. This category was clearly apparent in the DITN upper sensor (Fig. 6a), as one would expect to be the case where there is substantial summer surface water. However, and this is why it is highlighted here, it was also found at mid sensor at DITN and at DITS at both the upper and mid depths (Fig. 6e,f,g). In addition, the Category Two region is identified here ($S_A = 34.8$ –34.95 g kg⁻¹ and $\Theta = -1.9$ to -2.1 °C) and is TNBISW but notable because it is colder and more variable than the deeper samples. It was only clearly observed at DITS mid-water column and potentially could be recognized as south Drygalski ISW. The more tightly constrained TNBISW is based on comprehensive datasets to the north of the DIT and matches well with bottom sensor data. That the mid-depth DITS signal was outside this categorization highlights some differences between stations and hence between the north and south sides of the DIT.

Monthly averages of the currents at the mooring instrument

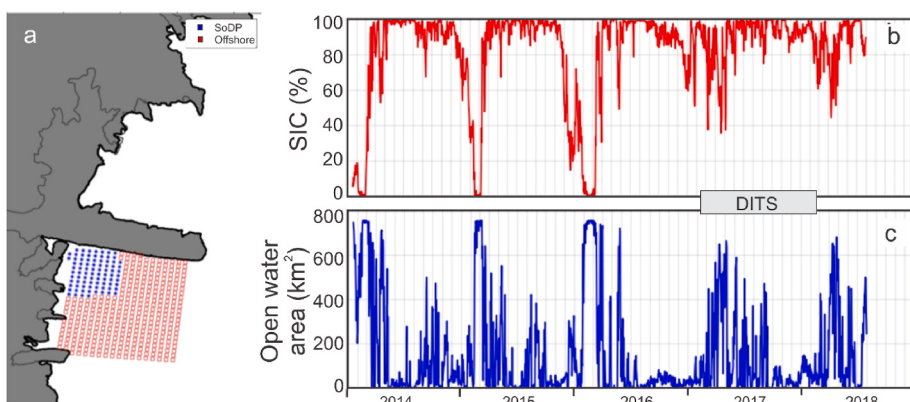


Fig. 4. Sea ice timeseries showing from (a) selected Southern Drygalski Polynya and offshore regions. From this, timeseries of (b) sea ice coverage and (c) polynya (open water) area are shown. The present DITS timeseries is marked in the grey box (b).

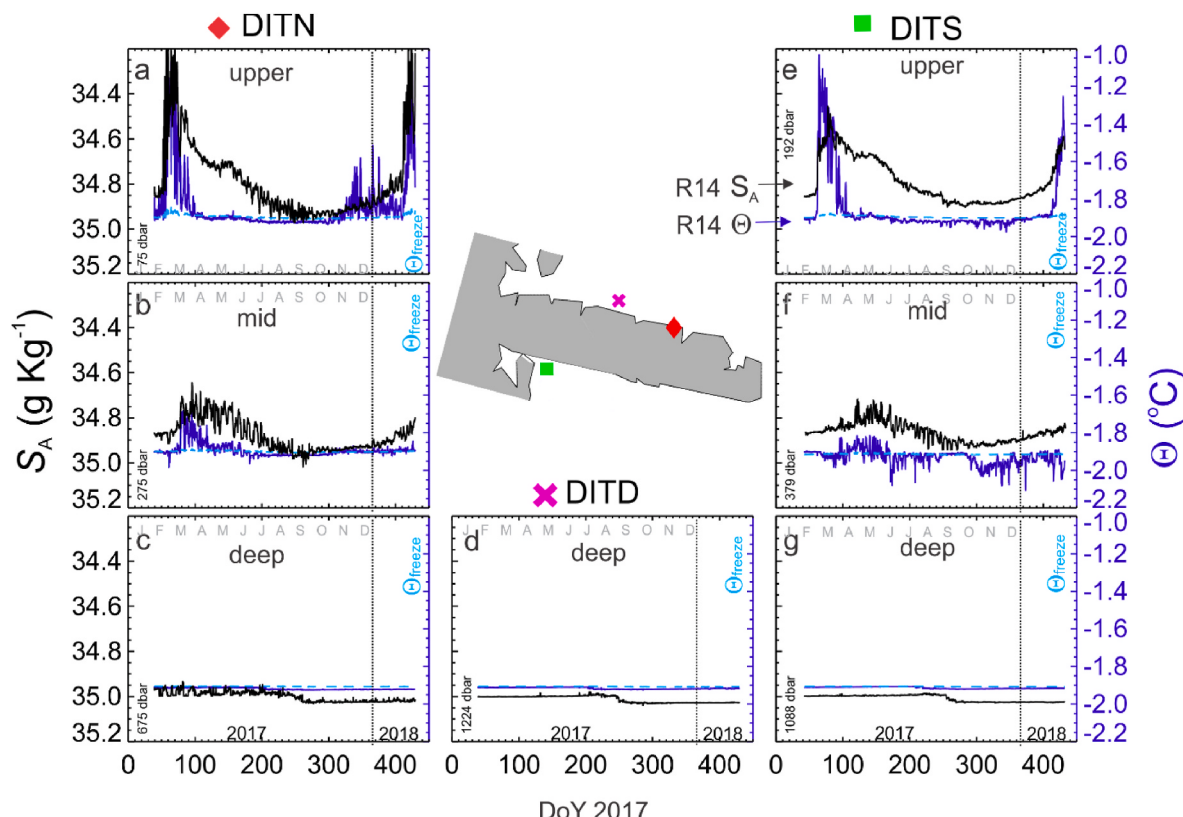


Fig. 5. Temperature and salinity (TEOS-10) timeseries structure (n.b. Here the salinity is shown as decreasing in the vertical to aid interpretation) for each mooring location DITN (a,b,c), DITD (d) and DITS (e,f,g). The R14 level in (e) identifies, for both temperature and salinity, more southerly surface water properties from Robinson et al. (2014). Surface freezing temperatures are also shown.

locations (Fig. 7) show the north-side mean flows at the upper and middle sensors moving northwestward (Fig. 7a) through to westward (Fig. 7b) which generally supports the summer snapshot of Yoon et al. (2020) derived from lowered current meter profiles. The equivalent moored current meter sensors on the south side (Fig. 7e and f) show flows were moving southward but slower. The near-bed sensor records are somewhat contradictory, with the north and south locations showing similar patterns through the year (Fig. 7c–g), but the deep station DITD (Fig. 7d) was flowing strongly northward. Recalling that these sensors are at different depths it implies southward circulation along the banks of the trough and clear northward flow in the very deepest of the trough.

3.3. Water column vertical structure

The summertime snapshot of vertical temperature structure (Fig. 8) at the three mooring stations shows warmer water constrained to the upper 300 m. Notably, the profile at DITS observed a ~280 m thick layer of presumably Ice Shelf Water at temperatures approaching the in situ freezing temperature (depth range 340–620 dbar – shaded in Fig. 8). Salinity was consistent between the three stations although DITS did have a very low salinity surface layer. Despite DITN water column being half the depth of DITD, at least at the time of the profiles, the near bed salinities were nearly the same.

In terms of variability in the frequency domain, Fig. 9 shows that the upper sensors at both stations see elevated temperature variability at the diurnal frequency but this is not seen at the deeper sensors. The deeper temperature at DITS has a similar spectral slope to the upper sensors but reaches its noise floor beyond around 10 cpd. The spectral slope for the DITS deeper sensor is different to the DITN equivalent (keeping in mind the sensor is 400 m deeper). The DITN deep sensor had elevated variability in the 0.1–5 cpd range and potentially is influenced by convection.

3.4. Glacial melt rates and meltwater fluxes

Glacial basal melting is a function of the turbulent heat flux from the ocean to the glacial ice. This can be calculated using near-ice ocean properties (McPhee, 2008). Here we use the mooring observation (temperature, salinity, depth and current speed) at three different layers as ocean properties at the ice-ocean interface at the corresponding depth. This needs to be treated with caution due to the complex bottom morphology of the Drygalski Tongue (Tabacco et al., 2000). The basal melting rate at different depths of the DITS mooring is listed in Table 2 by following the method described Stern et al. (2013) using a drag coefficient and the measured water temperature and salinity (drag coefficient 1.5×10^{-3} and bulk Stanton Number 0.0057). The five-day-average results based on the mooring data (Fig. 10) indicate that the basal melting close to DITS was strongest in the bottom layer. However, the annual basal melting at the bottom layer was only about $\sim 1.4 \text{ m a}^{-1}$, which cannot change the glacier geometry rapidly. This is close to the estimate from Gomez-Fell et al. (2023) of 1.46 m a^{-1} but less than 1.9 m a^{-1} from Adusumilli et al. (2020) – albeit with large uncertainty margin. However, examining the spatial distribution of the Adusumilli et al. (2020) melt rate this glacier average is driven by significant enhanced melting right in the corner by DITS, as well as generally larger melt rates on the south side (Fig. 2).

Since Terra Nova Bay is one of the most active source regions for HSSW production, the ocean water here is usually cold, which directly contributes to this low basal melting. The low basal melting at depth (between middle and bottom layer) likely aids the stability of David Glacier and Drygalski Ice Tongue. CTD profile data also provides an estimate of meltwater. The south-side CTD data suggests a meltwater flux estimated to be 0.25 mSv (or 8.0 Gt/year) which is comparable to 7.6 Gt/year estimate for the entire Drygalski region suggested in Rignot et al. (2013). This also supports the generally larger melt rates on the

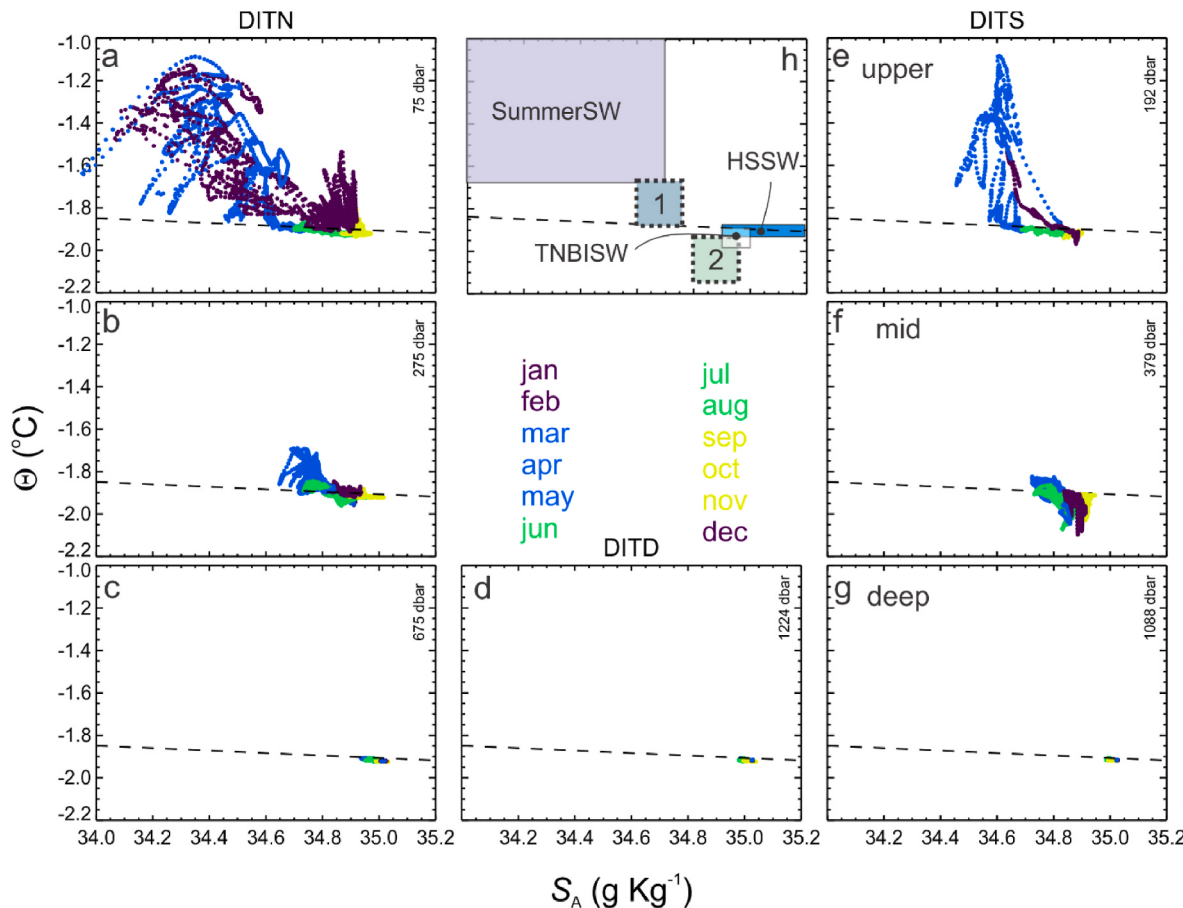


Fig. 6. Salinity vs Temperature (TEOS-10) for each mooring location DITN (a,b,c), DITD (d) and DITS (e,f,g) and colour-coded with season. Surface freezing temperatures are also shown. Panel (h) provides a water mass key following Budillon and Spezie (2000) with Summer Surface Water (Summer SW), Terra Nova Bay Ice Shelf Water (TNBISW) and High Salinity Shelf Water (HSSW). New categorisations, 1 and 2, are described in the text. Dashed line is surface freezing temperature.

south side (Fig. 2).

4. Discussion

HSSW in the Terra Nova Bay region is expected to be around $\Theta \sim -1.91^\circ\text{C}$, $34.9 < S_A \text{ g Kg}^{-1}$ (Budillon and Spezie, 2000 converted to TEOS-10) and this was seen consistently at the near-bed sensors at all stations and for around half the year at the mid-depth stations. It was seen at the upper sensors only sporadically at DITS, whereas at DITN it persisted over the July–December period. Clearly there were hydrographic differences between south and north of the DIT. The near-bed temperature and salinity properties (Fig. 11) prove to be useful in highlighting different regimes through the year (recalling that the sensors are at different depths). This provides an explanation for why the shallowest sensor, DITN, provides the lower bound for salinity.

Although near-bed temperature and salinity at DITN were highly variable (Fig. 11), the peaks in salinity at DITN provide a clear lower salinity bound for the DITS and DITD. Furthermore, the lowest salinity observed in the entire annual cycle at DITS occurred just after the DITS temperature drop. Temperature differences between the stations in Fig. 11 is comparable to instrument accuracy so likely not meaningful. The difference in sensor depth for the “deep” sensors helps explain why there appears to be a southward propagation in signal, but the current at the deepest location is northward. The connection “pathways” between DITN and DITS and DITN and DITD are likely separate. Notably, the year-long records do not “wrap-around” at their limits as there is year-year variability (Yoon et al., 2020).

Considering water masses previously described in the region by

Budillon and Spezie (2000) as summer surface water, Terra Nova Bay Ice Shelf Water and HSSW, it would appear we observed two perturbations on these categories. For much of the austral autumn, water observed at mid-depth at DITN (Fig. 6b) that sat between the ice-affected waters and the surface waters (“Category One” in Fig. 6h). Given that this is below the depth at which the warming occurs and primarily seen in the Autumn, it is presumably the mixing down of the summer surface waters. In addition, the colder “Category Two” Ice Shelf Water was observed (Fig. 6h) at mid-depth at DITS (Fig. 6f) and persists through the year. There is evidence that some of this water mass exits to the north (Fig. 6b) and ISW from the Nansen Ice Shelf has been observed in hydrographic survey work (Yoon et al., 2020). However, the present data suggest that there was a source of sub-surface ISW to the south of the DIT (340–620 dbar in Fig. 8) although there is nothing to indicate that this was the same source as that seen at DITN. It could be from as far south as the Ross/Mcmurdo ice shelves, although diffusive arguments suggest it would only be weakly separable from the local conditions (Hughes et al., 2014). Alternately, it might be produced locally with the Cheetham and Drygalski glacier tongues and Nansen Ice Shelf and Priestley Glacier nearby (Fig. 1).

Focusing on the deep temperature and salinity records either side of the DIT (Fig. 11), there are some key points to examine. The deep temperature and salinity signals at all stations were reasonably similar, although the DITN salinity was very variable. Furthermore, there was a lag of 8–9 days between DITN and DITS based on transient events seen in the temperature and salinity structure. There are two ways of viewing such a lag either (1) it is a direct transmission time from one location to the other, or (2), something that happens elsewhere arrives at the two

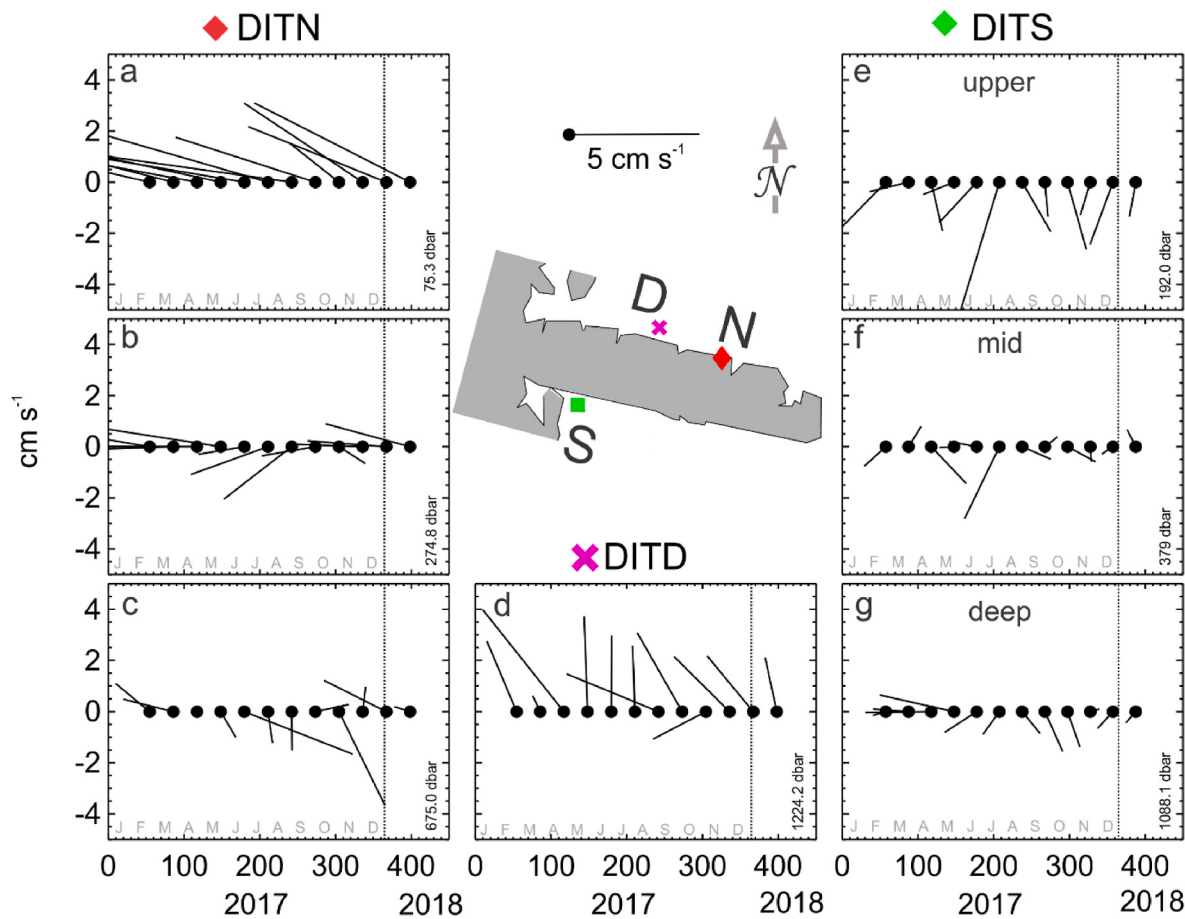


Fig. 7. Monthly-averaged currents for each mooring location DITN (a,b,c), DITD (d) and DITS (e,f,g) with the line pointing along the direction of flow.

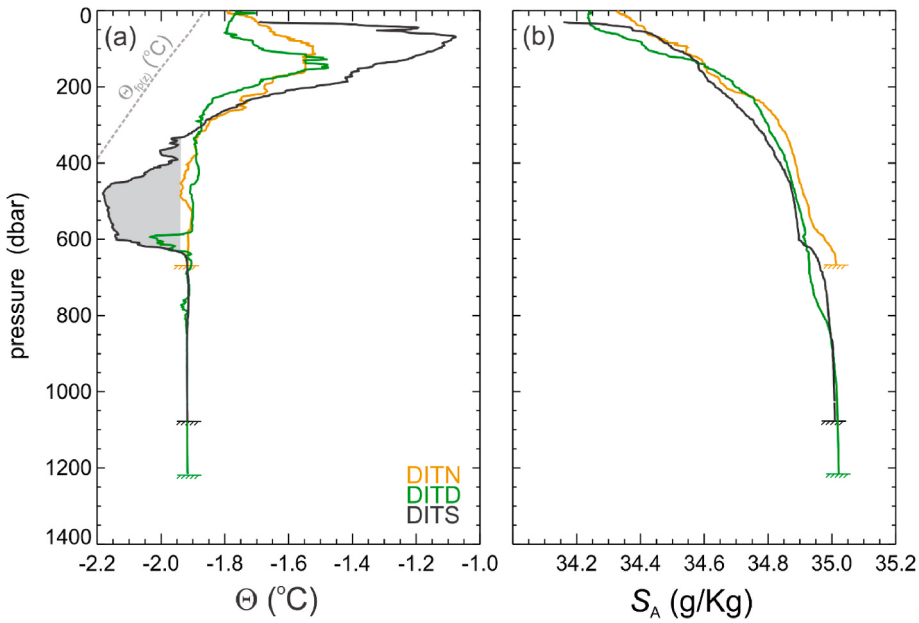


Fig. 8. CTD profiles from the three stations (TEOS-10) just after mooring recoveries (March 2018). The shaded section of the DITS profile shows the approximate basal-melt affected ISW layer.

locations at different times. If it is a direct travel, the lag implies a southward flow at deeper stations of around 5–6 cm s⁻¹ which is directionally possible but faster than suggested by the monthly current

averages at DITN and DITS (Fig. 7). Clearly, based on velocity, the signal at DITD was propagating northward so presumably the processes generating the transients happen elsewhere and entered the channel that

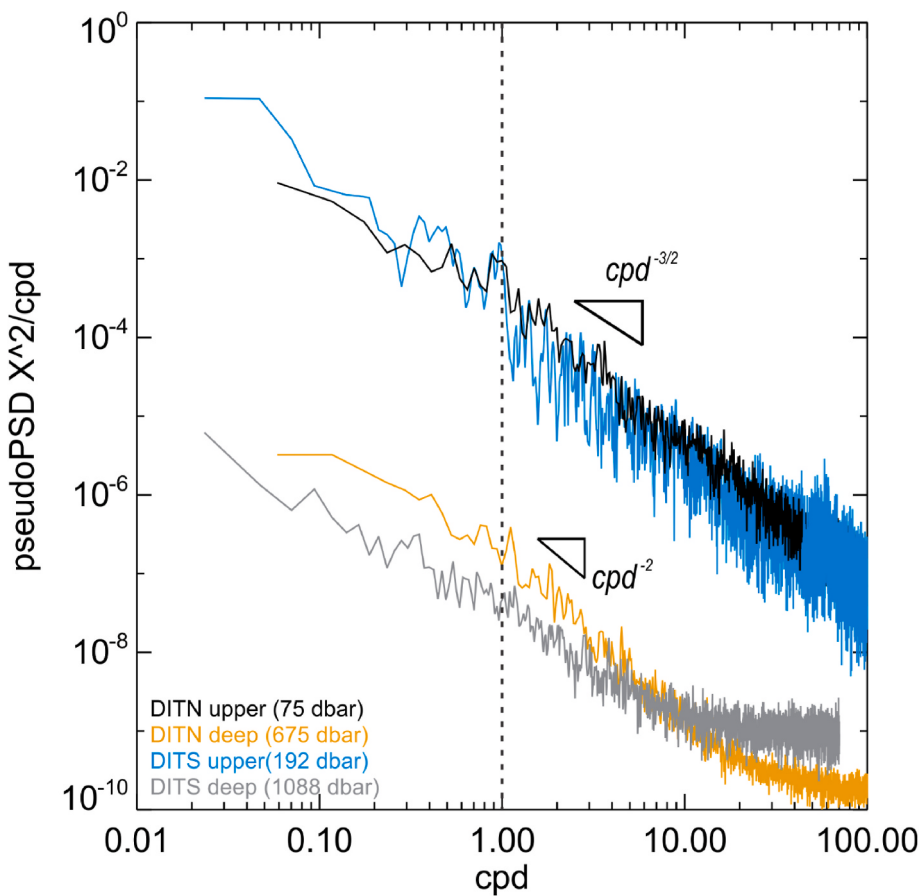


Fig. 9. Frequency structure from mooring temperature timeseries. The spectra are not offset, the differences between mean level of shallow and deep are due to differing background temperature gradients at the different depths.

Table 2

Basal melting rate (five-day average) calculated from DITS mooring observations. The max and mean melting rates at three different layers corresponding to the observation period are listed below. The error bands are the standard deviation of the melt rate. Positive value indicates basal melting.

DITS Layer	Melting_Rate_Mean (m/a)	Melting_Rate_Max (m/a)
Top (192 dbar)	0.43 ± 0.39	2.41 ± 1.10
Middle (379 dbar)	0.69 ± 0.33	2.41 ± 1.28
Bottom (1088 dbar)	1.36 ± 0.53	2.97 ± 1.70

holds DITS.

The sharp changes in temperature led those in salinity by around 40 days (Fig. 11). The implication is that the temperature change is when the local water column becomes dominated by penetrative convection. This doesn't mean it is well-mixed as the salinity differential remains. The timing of this matches when the upper temperature at DITN dropped below the surface freezing temperature. As transients in the south lagged their appearance in the north, the DITS showed no isohaline conditions and the average currents at depth at DITN pointed southward. This suggests the convectively cooled conditions were happening in the north and flowing south. Forty days later (day 255), a step-like increase of nearly 0.04 g is seen in all three traces. There was no corresponding shift in upper sensor signals around this time, so we speculate that this was when sea ice production-induced salinity changes (e.g. Rusciano et al., 2013) reached the sea floor. It is also the point at which upper water column salinity variability ceases (Fig. 3).

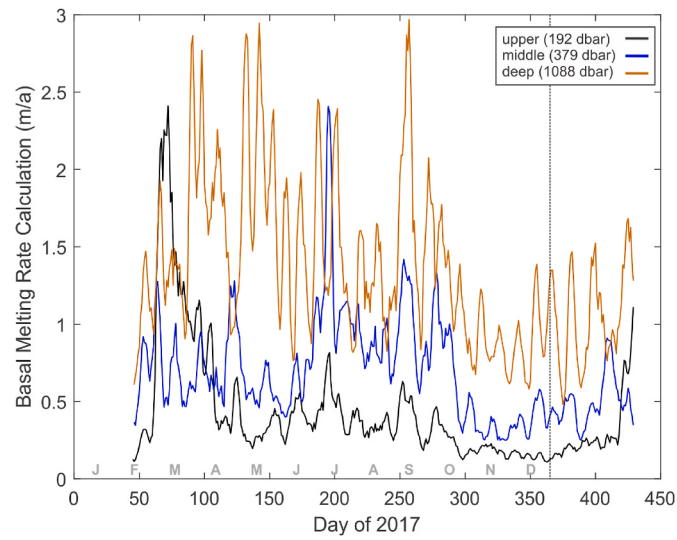


Fig. 10. Basal melting calculation from three different layers (shallow, middle, and deep) using mooring data from DITS. The curves indicate the five-day averaged basal melting results.

4.1. What drives the water column to the south of the Drygalski Ice Tongue?

The water column on the south side of the Drygalski will be influenced by some combination of local scales through polynya processes or

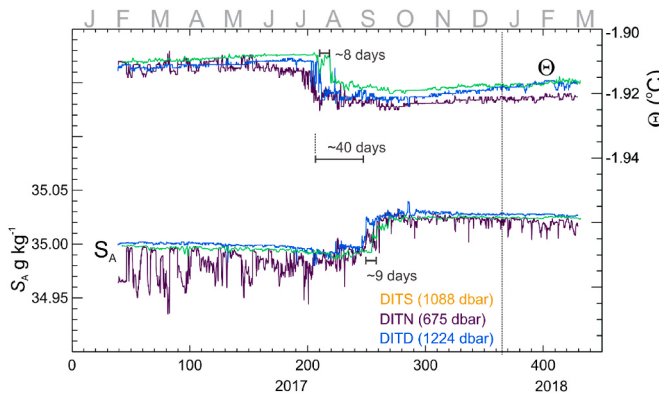


Fig. 11. Timeseries of near-bed potential temperature and salinity (TEOS-10) behaviour at the three mooring sites. The sample stations are at different depths. Temporal lags are marked for key transitions in both temperature and salinity as well as between the two records.

meltwater inputs, or more widely from regional circulation. Remotely sensed data confirm a Southern Drygalski Polynya that intermittently operates in the March–September period but abruptly shuts in mid-winter. This confirms the surface expression identified in Nihashi et al. (2023). The conjecture here is that the polynya's ability to open is affected by the regional sea ice (Gomez-Fell et al., 2023) and by mid-winter there is sufficient consolidated sea ice in the south DIT region that no matter how strong the off-continent katabatic wind gets, the polynya cannot open (Fraser et al., 2021). This is supported by the relationship between Southern Drygalski open water area and sea ice concentration in the offshore region (Fig. 4) which shows how a reduction in offshore sea ice enables the polynya area to open. The connection between the two records is tightly coupled with even the fine structure in the offshore sea ice being reflected in the inner open water area. The uppermost averaged currents flow southward, most likely as a recirculation due to the ice tongue. This would serve to aid the polynya opening. Finer-resolution polynya determination might potentially improve this conclusion (Burada et al., 2023). However, the HSSW structure does not support local HSSW production as the upper record at DITS does not identify this water mass. Despite this, HSSW is observed at mid and deep records. This suggests inflow from the north beneath the ice tongue.

4.2. Are DITN and DITS water column locations connected?

These data suggest there is an oceanic connection between the north and south sides of the DIT and that the DIT provides no physical barrier at depth. The initial hypothesis that northward flow along the coast broadly moves water from south to north is however not supported by the data. Critically, the monthly-averaged velocities at the DITS location are almost all southward. It could well be that there is some localized behaviour in the region inshore of DITS as suggested by basal melt (Fig. 2). Also, the lag between deep transients suggests the connection is from north to south, but this cannot be a general conclusion as the DITS hydrography exhibited some conditions not seen at the DITN.

In terms of north-south connection there are three depth-based components. The first is surface water. The strongly northwestward “surface” flow at DITN (seen in van Woert et al., 2001 also) could still be entraining water from the south side, possibly via some eddy process (Friedrichs et al., 2022). The initial working hypothesis was that the south Drygalski polynya-affected ocean might then affect the larger TNBP. The indication that the DIT forms a barrier to northward propagation of ISW from the Ross Ice Shelf (Stevens et al., 2017) suggests that we should see colder, fresher water at the surface. Robinson et al. (2014) observed surface water properties further south (latitude 77° 40' S) in the range -1.93 ± 0.02 °C and 34.8 ± 0.02 g kg⁻¹. This combination of

properties certainly is found in the DITS upper sensor data (Fig. 5e), but these continually evolve through the year and a range of conditions were seen.

The second, mid-water, aspect of north-south connection is the water at mid-depth is entrained by polynya operation. If this contains ISW (which it does at DITN) and then entrained into surface water, it likely accelerates sea ice formation (see next subsection). However, it appears more likely that there is a pathway for both north-side generated HSSW and ISW to be present in the water column on the south-side. The 2014 hydrographic survey (Stevens et al., 2017) observed that the southwest corner structure (i.e. DITS region - Fig. 1b) beneath the surface warm, salty layer sustains a block of very cold water extending to 200 m depth along with a distinct layer at 370 m of water at $\theta_0 \sim -1.93$ °C however, these conditions not seen in these data. As this class of ISW is not seen to the north there is the possibility that this accumulated against the south wall of the DIT and acts as a local heat sink. Robinson et al. (2014) identified RISC outflow of around $\Theta \sim -1.95$ °C and $S_A = 34.8$ g kg⁻¹. If this was the source, it had subducted beneath lighter waters as it is seen at the surface further south on the western side of McMurdo Sound (Robinson et al., 2014). The monthly-average current vectors imply southward flow, however there will have to be some form of recirculation due to the cryotopographic barrier caused by the DIT. The final pre-conditioning pathway is near the seabed whereby, if all the near-bed water in the deeper trough region (Fig. 7d) is flowing north, then HSSW formed at the south side polynya will augment and mix with that formed in TNBP proper.

4.3. Are there implications for TNBP and the local/regional ice shelf cavity circulation?

It is useful to place the 2017 results in a wider inter-annual context. Yoon et al. (2020) and Brett et al. (2020) both identified 2017 as a windy year in the Ross Sea with high occurrence of the Terra Nova Bay, and Ross Sea and McMurdo Sound polynyas. This led to very thick pack ice the western Ross Sea (Rack et al., 2021). In terms of Antarctic sea ice extent, the 2016/2017 summer season, when some of these observations were taken, was regarded as low. Stuecker et al. (2017) and Turner et al. (2017) identified that the, at the time, unprecedented minimum in sea ice extent occurred from November 2016 to April 2017 and was concentrated mainly in Weddell and Ross Seas. Despite these departures, Miller et al. (2024a) found that Terra Nova Bay HSSW for 2017 was comparable to the longer-term average.

The presence and advection of ISW is important also for sea ice formation. While studies have suggested far-field ISW sources (e.g. Robinson et al., 2014), the nearby melt identified in Figs. 2 and 10 suggest local sources of this ISW. Category Two near-ISW is clearly seen at DITS (Fig. 6). It may have come from (i) the TNBP region by flowing southward around the DIT, (ii) via direct melting of the basal region of the DIT, (iii) from the David-Drygalski grounding zone or (iv) from a south-side ice shelf cavity. Yoon et al. (2020) observed ISW between 200 and 700 m depth in CTD profiles well to the north of the DIT, close to the Hell's Gate ice shelf and the northern extent of the Nansen. Similarly, Miller et al. (2024a) observed ISW at 47 m depth in moored data (see Fig. 1) close by the location of the Yoon et al. (2020) results. This ISW signal could come from nearby ice shelves and ice tongues (e.g. Tison et al., 1993). This was not strongly reflected in the DITN data further south in the TNBP, but it is possible that the ISW layer sat between the middle and bottom sensors at this location.

The presence of an ISW plume potentially provides an additional heat-sink (Fig. 12) in addition to the wind-driven cooling at the surface. This has some parallels with supply of heat by circumpolar deep water as an internal source for the heat budget (Fusco et al., 2009). Thermodynamic approaches to polynya behaviour require quantification of the vertical entrainment velocity W_e (Lemke, 1987; Sansiviero et al., 2017) which can be thought of as being a convective velocity scale w^* . Scaling implies $w^* = 0(Bh_c)^{1/3}$ where B is the buoyancy flux and h_c is the vertical

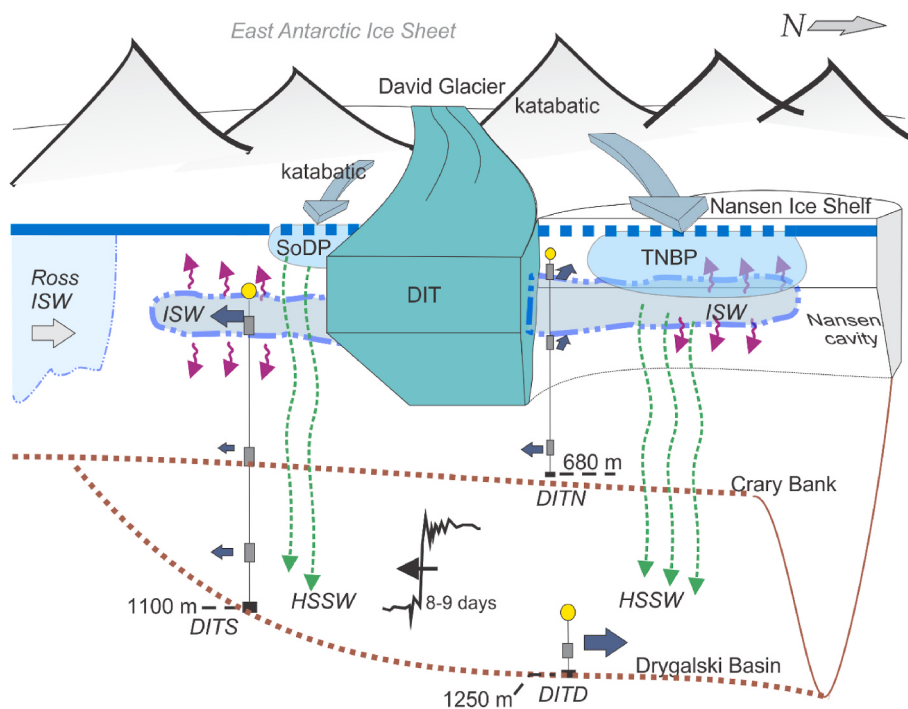


Fig. 12. Synthesis sketch looking westward towards the land showing major cryotopographic features including the DIT, Nansen Ice Shelf and sea ice, along with the katabatic-driven TNBP. Also shown are the Ice Shelf Water (ISW) layer and mooring locations. In order to aid the interpretation, the sketch distorts the view as it is not to exact scale and it doesn't make clear that the DIT grounding line is actually well inshore of the coast and deeper than the neighboring ocean.

convective scale (Table 3). With surface heat fluxes around -150 W m^{-2} . (e.g. Fusco et al., 2009) acting over an area of around $20 \times 30 \text{ km}$, indicates around 10^{10} W . An ISW plume with a thermal deficit of $\Delta\Theta = 0.2^\circ \text{C}$ propagating at say $u_{ISW} = 5 \text{ cm s}^{-1}$, although Buffoni et al. (2002) suggest more like 1 cm s^{-1} , over a depth of $\delta = 200 \text{ m}$ and some width L_{ISW} removes $\delta L_{ISW} u_{ISW} \rho_0 c_p \Delta\theta$ from the system. This suggests the ISW plume would have to be around 11.5 km wide to provide the same effect as the surface heat flux. This scale is entirely possible and suggests that ISW plumes could play a significant role in the heat balance in polynya regions. The supply is modulated by the surface processes. It was expected that this ISW would have a fresher signal than the water around it, but as salinity effectively controls density this is not the case and the ISW in Fig. 8 is only slightly fresher than the neighboring profiles.

If the aggregating cooler water, both from the south at the surface, or locally sourced ISW, is able to be entrained into the surface waters of the TNBP, it will precondition the polynya by requiring less cooling and also higher initial upper ocean stratification to contain the initial wind-driven cooling. This suggests the ratio of heat lost to the ISW plume vs the surface fluxes form a preconditioning parameter based on typical polynya area and heat flux relative to the supply of cooler, fresher water ISW. This requires improved knowledge of the source and pathways of ISW in the region.

Table 3
Heat flux calculations.

Quantity	Example values	dimensions
B, buoyancy flux $g\alpha Q_H / (c_p \rho_0)$	–	$\text{m}^2 \text{s}^{-3}$
h_c , vertical convective scale – effectively the water column depth	nominal 1000 m	m
α , coefficient of thermal expansion	2.5×10^{-5} for $S = 34.6 \text{ psu}$ and $\theta = -1.9^\circ \text{C}$	$^\circ \text{C}^{-1}$
C_p , specific heat capacity of seawater	4×10^3	$\text{J kg}^{-1} \text{ }^\circ \text{C}^{-1}$
ρ_0 , reference density	1028	kg m^{-3}
Q_H heat flux	-150	W m^{-2}

5. Conclusions

New hydrographic data from the south side of the large Drygalski Ice Tongue add key elements to our understanding of regional circulation and the role of glaciers and polynyas. The south side of the ice tongue is known to be melting faster than the north side. The temperature and salinity data exhibit clear differences to that measured close by, but on the north side of the ice tongue. Subsurface ISW is observed and is sufficiently cold as to influence polynya operation, such that ISW might be considered a “pre-conditioner” of polynya. Furthermore, transients in near-bed temperature and salinity were observed on both sides of the ice tongue. However, there were temporal offsets depending on location and temperature transients preceded that of salinity. Current measurements at this near-coastal position suggests the circulation beneath the ice tongue is primarily southward. The data illustrate the complex interplay between polynya and ocean behaviour and provide a useful counterpoint to the extensive observations to the north of the ice tongue.

CRediT authorship contribution statement

Craig Stevens: Writing – original draft, Resources, Project administration, Methodology, Investigation, Funding acquisition, Formal analysis, Conceptualization. **Seung-Tae Yoon:** Writing – original draft, Methodology, Investigation, Conceptualization. **Christopher J. Zappa:** Investigation, Conceptualization. **Una Kim Miller:** Writing – review & editing, Investigation. **Xianwei Wang:** Methodology, Investigation. **Fiona Elliott:** Methodology, Data curation, Conceptualization. **Liv Cornelissen:** Validation, Data curation. **Choon-Ki Lee:** Investigation, Conceptualization. **Sukyoung Yun:** Investigation, Data curation. **Won Sang Lee:** Resources, Project administration, Funding acquisition, Conceptualization.

Declaration of competing interest

The authors declare that they have no known competing financial interests or personal relationships that could have appeared to influence

the work reported in this paper.

Data availability

The data are available through the Korea Polar Data Centre.

Acknowledgements

The authors wish to acknowledge the support of the Korea Polar Research Institute (PM16020), the New Zealand Antarctic Research Institute, New Zealand Deep South National Science Challenge and the MBIE Antarctic Science Platform (ANTA 1801). We thank Brett Grant, Jasmin McInerney, Sarah Searson, Mike Brewer, Alex Forrest, Pierre Dutrieux, and Gary Wilson for their support and advice. Christine Dow is thanked for discussion on the David Glacier grounding line. Xianwei Wang was supported by National Natural Science Foundation of China (Grant No. 42276237) and the Oceanic Interdisciplinary Program of Shanghai Jiao Tong University (No. SL2022PT205). Seung-Tae Yoon and Won Sang Lee were supported by the Korea Institute of Marine Science & Technology Promotion (KIMST) funded by the Ministry of Oceans and Fisheries (RS-2023-00256677). C. J. Zappa was supported by NSF Office of Polar Programs (OPP) awards 1341688 and 2332418. U. K. Miller was supported by National Aeronautics and Space Administration (NASA) award 80NSSC19K1348. Craig Stewart and two anonymous reviewers are thanked for constructive comments on the initial draft. The staff at Jang Bogo Station, the crew of the RV *Araon*, KOPRI and Antarctica New Zealand are thanked for their operational support. The DITS mooring had been scheduled to be recovered by RV *Araon* during ANA09B however it was inaccessible under fast ice. The eventual recovery was carried out on the Italian icebreaker RV *Laura Bassi* on January 29, 2020 thanks to the efforts of Drs Pierpaolo Falco, Pasquale Castagno and PNRA (Programma Nazionale di Ricerche in Antartide). We acknowledge the use of Rapid Response imagery from the Land, Atmosphere Near real-time Capability for EOS (LANCE) system operated by the NASA/GSFC/Earth Science Data and Information System (ESDIS) with funding provided by NASA/HQ. Wind data were obtained from ‘MeteoClimatological Observatory at MZS and Victoria Land’ of the Italian PNRA. Hydrographic data are available via the Korea Polar Data Centre (kpdc.kopri.re.kr).

References

- Adusumilli, S., Fricker, H.A., Medley, B., Padman, L., Siegfried, M.R., 2020. Interannual variations in meltwater input to the Southern Ocean from Antarctic ice shelves. *Nat. Geosci.* 13, 616–620. <https://doi.org/10.1038/s41561-020-0616-z>, 2020.
- Aulicino, G., Sansiviero, M., Paul, S., Cesaroni, C., Fusco, G., Wadhams, P., Budillon, G., 2018. A new approach for monitoring the Terra Nova Bay polynya through MODIS Ice Surface Temperature Imagery and its validation during 2010 and 2011 winter seasons. *Rem. Sens.* 10, 366. <https://doi.org/10.3390/rs10030366>.
- Bennetts, L.G., Shakespeare, C.J., Vreugdenhil, C.A., Foppert, A., Gayen, B., Meyer, A., et al., 2024. Closing the loops on Southern Ocean dynamics: from the circumpolar current to ice shelves and from bottom mixing to surface waves. *Rev. Geophys.* 62, e2022RG000781 <https://doi.org/10.1029/2022RG000781>.
- Bowen, M.M., Fernandez, D., Forcen-Vazquez, A., Gordon, A.L., Huber, B., Castagno, P., Falco, P., 2021. The role of tides in bottom water export from the western Ross Sea. *Sci. Rep.* 11 (1), 1–11. <https://doi.org/10.1038/s41598-021-81793-5>.
- Brett, G.M., Irvin, A., Rack, W., Haas, C., Langhorne, P.J., Leonard, G.H., 2020. Variability in the distribution of fast ice and the sub-ice platelet layer near McMurdo Ice Shelf. *J. Geophys. Res.: Oceans* 125 (3), e2019JC015678.
- Budillon, G., Cordero, S.G., Salusti, E., 2002. On the dense water spreading off the Ross Sea shelf (southern ocean). *J. Mar. Syst.* 35, 207–227. [https://doi.org/10.1016/S0924-7963\(02\)00082-9](https://doi.org/10.1016/S0924-7963(02)00082-9).
- Budillon, G., Spezie, G., 2000. Thermohaline structure and variability in the Terra Nova Bay polynya, Ross Sea. *Antarct. Sci.* 12 (4), 493–508. <https://doi.org/10.1017/S0954102000000572>.
- Buffoni, G., Cappelletti, A., Picco, P., 2002. An investigation of thermohaline circulation in the Terra Nova Bay polynya. *Antarct. Sci.* 14 (1), 83–92. <https://doi.org/10.1017/S0954102002000615>.
- Burada, G.K., McDonald, A., Renwick, J., Jolly, B., 2023. Delineating polynya area using active and passive microwave sensors for the Western Ross Sea sector of Antarctica. *Rem. Sens.* 15 (10), 2545. <https://doi.org/10.3390/rs15102545>.
- Cappelletti, A., Picco, P., Peluso, T., 2010. Upper ocean layer dynamics and response to atmospheric forcing in the Terra Nova Bay polynya, Antarctica. *Antarct. Sci.* 22 (3), 319–329. <https://doi.org/10.1017/S095410201000009X>.
- Castagno, P., Capozzi, V., DiTullio, G.R., Falco, P., Fusco, G., Rintoul, S.R., Spezie, G., Budillon, G., 2019. Rebound of shelf water salinity in the Ross Sea. *Nature Commun.* 10 (1), 5441.
- Ciappa, A., Pietranera, L., Budillon, G., 2012. Observations of the Terra Nova Bay (Antarctica) polynya by MODIS ice surface temperature imagery from 2005 to 2010. *Remote Sens. Environ.* 119, 158–172. <https://doi.org/10.1016/j.rse.2011.12.017>.
- Dee, D.P., Uppala, S.M., Simmons, A.J., Berrisford, P., Poli, P., Kobayashi, S., Andrae, U., Balmaseda, M.A., Balsamo, G., Bauer, D.P., Bechtold, P., 2011. The ERA-Interim reanalysis: configuration and performance of the data assimilation system. *Q. J. Roy. Meteorol. Soc.* 137 (656), 553–597.
- Dow, C.F., Lee, W.S., Greenbaum, J.S., Greene, C.A., Blankenship, D.D., Poinar, K., Forrest, A.L., Young, D.A., Zappa, C.J., 2018. Basal channels drive active surface hydrology and sub-ice shelf fracture. *Sci. Adv.* 4 (6), eaao7212.
- Fraser, A.D., Massom, R.A., Handcock, M.S., Reid, P., Ohshima, K.I., Raphael, M.N., Cartwright, J., Klekociuk, A.R., Wang, Z., Porter-Smith, R., 2021. Eighteen-year record of circum-Antarctic landfast-sea-ice distribution allows detailed baseline characterisation and reveals trends and variability. *Cryosphere* 15, 5061–5077. <https://doi.org/10.5194/tc-15-5061-2021>.
- Frezzotti, M., Mabin, M.C.G., 1994. 20th century behaviour of Drygalski ice tongue, Ross Sea, Antarctica. *Ann. Glaciol.* 20, 397–400. <https://doi.org/10.3189/172756494794587492>.
- Friedrichs, D.M., McInerney, J.B., Oldroyd, H.J., Lee, W.S., Yun, S., Yoon, S.T., Stevens, C.L., Zappa, C.J., Dow, C.F., Mueller, D., Sepulveda Steiner, O., 2022. Observations of submesoscale eddy-driven heat transport at an ice shelf calving front. *Communications Earth & Environment* 3 (1), 140.
- Fusco, G., Budillon, G., Spezie, G., 2009. Surface heat fluxes and thermohaline variability in the Ross Sea and in Terra Nova Bay polynya. *Continent. Shelf Res.* 29, 1887–1895. <https://doi.org/10.1016/j.csr.2009.07.006>.
- Fusco, G., Flocco, D., Budillon, G., Spezie, G., Zambianchi, E., 2002. Dynamics and variability of Terra Nova Bay polynya. *Mar. Ecol. Prog. Ser.* 23, 201–209. <https://doi.org/10.1111/j.1439-0485.2002.tb00019.x>.
- Gomez-Fell, R., Marsh, O.J., Rack, W., Wild, C.T., Purdie, H., 2023. Basal mass balance and prevalence of ice tongues in the Western Ross Sea. *Front. Earth Sci.* 11, 1057761 <https://doi.org/10.3389/feart.2023.1057761>.
- Gunn, K.L., Rintoul, S.R., England, M.H., Bowen, M., 2023. Recent reduced abyssal overturning and ventilation in the Australian Antarctic Basin. *Nat. Clim. Change* 13, 537–544. <https://doi.org/10.1038/s41558-023-01667-8>.
- Hughes, K.G., Langhorne, P.J., Leonard, G.H., Stevens, C.L., 2014. Extension of an Ice Shelf Water plume model beneath sea ice with application in McMurdo Sound, Antarctica. *J. Geophys. Res.: Oceans* 119 (12), 8662–8687.
- Indrigo, C., Dow, C.F., Greenbaum, J.S., Morlighem, M., 2021. Drygalski Ice Tongue stability influenced by rift formation and ice morphology. *J. Glaciol.* 67 (262), 243–252. <https://doi.org/10.1017/jog.2020.99>.
- Jones, R.W., Renfrew, I.A., Orr, A., Webber, B.G.M., Holland, D.M., Lazzara, M.A., 2016. Evaluation of four global reanalysis products using in situ observations in the Amundsen Sea Embayment, Antarctica. *J. Geophys. Res. Atmos.* 121 (11), 6240–6257.
- Kusahara, K., Hasumi, H., Tamura, T., 2010. Modeling sea ice production and dense shelf water formation in coastal polynyas around East Antarctica. *J. Geophys. Res.* 115, C10006. <https://doi.org/10.1029/2010JC006133>.
- Lemke, P., 1987. A coupled one-dimensional sea ice-ocean model. *J. Geophys. Res.: Oceans* 92 (C12), 13164–13172.
- Lizotte, M.P., 2001. The contributions of sea ice algae to Antarctic marine primary production. *Am. Zool.* 41 (1), 57–73.
- Malyarenko, A., Robinson, N.J., Williams, M.J.M., Langhorne, P.J., 2019. A wedge mechanism for summer surface water inflow into the Ross Ice Shelf Cavity. *J. Geophys. Res.: Oceans* 124 (2), 1196–1214.
- Mathiot, P., Jourdain, N.C., Barnier, B., Galée, H., Molines, J.M., Sommer, J.L., Penduff, T., 2012. Sensitivity of coastal polynyas and high-salinity shelf water production in the Ross Sea, Antarctica, to the atmospheric forcing. *Ocean Dynam.* 62, 701–723. <https://doi.org/10.1007/s10236-012-0531-y>.
- McPhee, M., 2008. Air-ice-ocean Interaction: Turbulent Ocean Boundary Layer Exchange Processes. Springer Science & Business Media.
- Miller, U.K., Zappa, C.J., Gordon, A.L., Yoon, S.-T., Stevens, C.L., Lee, W.S., 2024a. High salinity shelf water production in Terra Nova Bay, Ross Sea from high-resolution near-surface salinity observations. *Nat. Commun.* 15, 373. <https://doi.org/10.1038/s41467-023-43880-1>.
- Miller, U.K., Zappa, C.J., Gordon, A.L., Yoon, S.-T., Stevens, C.L., Cornelissen, L., Yun, S., Lee, W.S., 2024b. The coupling of winds, ocean turbulence, and high salinity shelf water in the Terra Nova Bay polynya. *Deep Sea Res. II – this issue*.
- Morales Maqueda, M.A., Willmott, A.J., Biggs, N.R.T., 2004. Polynya dynamics: a review of observations and modeling. *Rev. Geophys.* 42 (1) <https://doi.org/10.1029/2002RG000116>.
- Nishishi, S., Ohshima, K.I., Tamura, T., 2023. Reconstruct the AMSR-E-2 thin ice thickness algorithm to create a long-term time series of sea-ice production in Antarctic coastal polynyas. *Polar Science*, 100978. <https://doi.org/10.1016/j.polar.2023.100978>.
- Orsi, A.H., Johnson, G.C., Bullister, J.L., 1999. Circulation, mixing, and production of antarctic bottom water. *Prog. Oceanogr.* 43 (1), 55–109. [https://doi.org/10.1016/S0079-6617\(99\)00004-X](https://doi.org/10.1016/S0079-6617(99)00004-X).
- Orsi, A.H., Smethie Jr, W.M., Bullister, J.L., 2002. On the total input of Antarctic waters to the deep ocean: a preliminary estimate from chlorofluorocarbon measurements. *J. Geophys. Res.: Oceans* 107 (C8). <https://doi.org/10.1029/2001JC000976>, 31–1.

- Parkinson, C.L., Cavalieri, D.J., Gloersen, P., Zwally, H.J., Comiso, J.C., 1999. Arctic sea ice extents, areas, and trends, 1978–1996. *J. Geophys. Res.: Oceans* 104 (C9), 20837–20856.
- Rack, W., Price, D., Haas, C., Langhorne, P.J., Leonard, G.H., 2021. Sea ice thickness in the western Ross Sea. *Geophys. Res. Lett.* 48 (1), e2020GL090866.
- Rignot, E., Jacobs, S., Mouginot, J., Scheuchl, B., 2013. Ice-shelf melting around Antarctica. *Science* 341 (6143), 266–270.
- Rintoul, S.R., 2018. The global influence of localized dynamics in the Southern Ocean. *Nature* 558, 209–218. <https://doi.org/10.1038/s41586-018-0182-3>.
- Robinson, N.J., Grant, B.S., Stevens, C.L., Stewart, C.L., Williams, M.J.M., 2020. Oceanographic observations in supercooled water: protocols for mitigation of measurement errors in profiling and moored sampling. *Cold Reg. Sci. Technol.* 170, 102954 <https://doi.org/10.1016/j.coldregions.2019.102954>.
- Robinson, N.J., Williams, M.J.M., Stevens, C.L., Langhorne, P.J., Haskell, T.G., 2014. Evolution of a supercooled Ice Shelf Water plume with an actively growing subice platelet matrix. *J. Geophys. Res.: Oceans* 119, 3425–3446. <https://doi.org/10.1002/2013JC009399>.
- Rusciano, E., Budillon, G., Fusco, G., Spezie, G., 2013. Evidence of atmosphere–sea ice–ocean coupling in the Terra Nova Bay polynya (Ross Sea—Antarctica). *Continent. Shelf Res.* 61, 112–124. <https://doi.org/10.1016/j.csr.2013.04.002>.
- Sansiviero, M., Maqueda, M.A.M., Fusco, G., Aulicino, G., Flocco, D., Budillon, G., 2017. Modelling sea ice formation in the Terra Nova Bay polynya. *J. Mar. Syst.* 166, 4–25. <https://doi.org/10.1016/j.jmarsys.2016.06.013>.
- Schodlok, M.P., Menemenlis, D., Rignot, E.J., 2016. Ice shelf basal melt rates around Antarctica from simulations and observations. *J. Geophys. Res.: Oceans* 121 (2), 1085–1109.
- Spreen, G., Kaleschke, L., Heygster, G., 2008. Sea ice remote sensing using AMSR-E 89-GHz channels. *J. Geophys. Res.: Oceans* 113 (C2).
- Stern, A.A., Dinniman, M.S., Zagorodnov, V., Tyler, S.W., Holland, D.M., 2013. Intrusion of warm surface water beneath the McMurdo Ice Shelf, Antarctica. *J. Geophys. Res.: Oceans* 118 (12), 7036–7048.
- Stevens, C., Lee, W.S., Fusco, G., Yun, S., Grant, B., Robinson, N., Hwang, C.Y., 2017. The influence of the Drygalski Ice Tongue on the local ocean. *Ann. Glaciol.* 58 (74), 51–59.
- Stevens, C.L., Robinson, N.J., Williams, M.J., Haskell, T.G., 2009. Observations of turbulence beneath sea ice in southern McMurdo Sound, Antarctica. *Ocean Sci.* 5 (4), 435–445.
- Stewart, C.L., Christoffersen, P., Nicholls, K.W., Williams, M.J., Dowdeswell, J.A., 2019. Basal melting of Ross Ice Shelf from solar heat absorption in an ice-front polynya. *Nat. Geosci.* 12 (6), 435–440.
- Stuecker, M.F., Bitz, C.M., Armour, K.C., 2017. Conditions leading to the unprecedented low Antarctic sea ice extent during the 2016 austral spring season. *Geophys. Res. Lett.* 44, 9008–9019. <https://doi.org/10.1002/2017GL074691>.
- Tabacco, I.E., Bianchi, C., Chiappini, M., Zirizzotti, A., Zucccheretti, E., 2000. Analysis of bottom morphology of the David Glacier–Drygalski ice tongue, east Antarctica. *Ann. Glaciol.* 30, 47–51. <https://doi.org/10.3189/172756400781820624>.
- Tamura, T., Ohshima, K.I., Fraser, A.D., Williams, G.D., 2016. Sea ice production variability in Antarctic coastal polynyas. *J. Geophys. Res.: Oceans* 121 (5), 2967–2979.
- Tison, J.-L., Ronveaux, D., Lorrain, R.D., 1993. Low salinity frazil ice generation at the base of a small Antarctic ice shelf. *Antarct. Sci.* 5, 309–322. <https://doi.org/10.1017/S0954102093000409>.
- Turner, J., Phillips, T., Marshall, G.J., Hosking, J.S., Pope, J.O., Bracegirdle, T.J., Deb, P., 2017. Unprecedented springtime retreat of Antarctic sea ice in 2016. *Geophys. Res. Lett.* 44, 6868–6875. <https://doi.org/10.1002/2017GL073656>.
- Van Woert, M.L., Meier, W.N., Zou, C.Z., Archer, A., Pellegrini, A., Grigioni, P., Bertoia, C., 2001. Satellite observations of upper-ocean currents in Terra Nova Bay, Antarctica. *Ann. Glaciol.* 33, 407–412. <https://doi.org/10.3189/172756401781818879>.
- Van Woert, M.L., 1999. Wintertime dynamics of the Terra Nova Bay polynya. *J. Geophys. Res.: Oceans* 104 (C4), 7753–7769.
- Williams, G.D., Bindoff, N.L., Marsland, S.J., Rintoul, S.R., 2008. Formation and export of dense shelf water from the Adélie Depression, East Antarctica. *J. Geophys. Res.: Oceans* 113 (C4).
- Xu, Y., Zhang, G., Maksym, T., Ji, R., Li, Y., 2023. Stratification breakdown in antarctic coastal polynyas. Part II: influence of an ice tongue and coastline geometry. *J. Phys. Oceanogr.* 53, 2069–2088. <https://doi.org/10.1175/JPO-D-22-0219.1>.
- Yoon, S.T., Lee, W.S., Stevens, C., Jendersie, S., Nam, S., Yun, S., Hwang, C.Y., Jang, G.I., Lee, J., 2020. Variability in high-salinity shelf water production in the Terra Nova Bay polynya, Antarctica. *Ocean Sci.* 16 (2), 373–388. <https://doi.org/10.5194/os-16-373-2020>.